Mon. Not. R. Astron. Soc. **000**, 1–?? (2008) Printed 22 May 2009 (MN LATEX style file v2.2)

IC10: the history of the nearest starburst galaxy through its Planetary Nebula and H II region populations ⋆

Laura Magrini[1]†; Denise R. Gonçalves[2]
[1] *INAF - Osservatorio Astrofisico di Arcetri, Largo E. Fermi 5, I-50125 Firenze, Italy*
[2] *UFRJ - Observatório do Valongo, Ladeira Pedro Antonio 43, 20080-090 Rio de Janeiro, Brazil*

Accepted ?. Received ?; in original form ?

ABSTRACT

We report the results of spectroscopic observations, obtained with the Gemini North Multi-Object Spectrograph, of 9 planetary nebulae (PNe) and 15 H II regions located in the $5.5'\times5.5'$ inner region of the nearby starburst galaxy IC10. Twelve new candidate PNe have been discovered during our pre-imaging phase. Nine of them have been spectroscopically confirmed. The direct availability of the electron temperature diagnostics in several nebulae allowed an accurate determination of the metallicity map of IC10 at two epochs: the present-time from H II regions and the old/intermediate-age from PNe. We found a non-homogeneous distribution of metals at both epochs, but similar average abundances were found for the two populations. The derived age-metallicity relation shows a little global enrichment interpreted as the loss of metals by SN winds and to differential gas outflows. Finally, we analyzed the production of oxygen –through the third dredge-up– in the chemical abundance patterns of the PN populations belonging to several dwarf irregular galaxies. We found that the third dredge-up of oxygen is a metallicity dependent phenomenon occurring mainly for $12+\log(O/H)\leqslant7.7$ and substantially absent in IC10 PNe.

Key words: Galaxies: abundances - evolution - Local Group - Individual (IC10); ISM: HII regions-Planetary Nebulae

1 INTRODUCTION

The irregular galaxy IC10 is the nearest starburst galaxy, sometimes defined as the closest example of a blue compact dwarf (Richer et al. 2001). It is located in the outskirts of the Local Group (LG), at low Galactic latitude. Its location implies quite uncertain determinations of its reddening and distance. The estimates of the reddening range from E(B-V)=0.47 to 2.0, while the distance modulus from 22 to more than 27 mag, i.e. the linear distance of the galaxy would vary from 0.5 to 3 Mpc (Sakai, Madore & Freedman 1999 and Demers, Battinelli & Letarte 2004, for a summary of distances and reddening). Recent estimations locate this galaxy at a distance around 0.7-0.8 Mpc (e.g. Demers et al. 2004; Kniazev, Pustilnik & Zucker 2008; Sanna et al. 2008).

IC10 is remarkable for many reasons: *i)* its high star formation rate (SFR), as evidenced by its large number of H II regions (Hodge & Lee 1990), Hα luminosity (Mateo 1998), and far-IR luminosity (Melisse & Israel 1994); *ii)* its huge number of Wolf-Rayet stars per unit luminosity, the largest in the LG (Massey, Armandroff & Conti 1992; Massey & Armandroff 1995), and the anomalous ratio of carbon-type Wolf-Rayet stars (WC stars) to nitrogen-type Wolf-Rayet stars (WN stars) which is peculiar at its metallicity (0.2–0.3 solar; cf. Skillman, Kennicutt& Hodge 1989 and Garnett 1990); *iii)* the presence of an extended, complex and counter-rotating envelope (Shostak & Skillman 1989) revealed by H I observations, which leads Wilcots & Miller (1998) to conclude that IC10 is still in its formative stage. All these characteristics suggest that IC10 is experiencing an intense and very recent burst of star formation, starting about 10 Myr ago.

Several studies in IC10 have revealed the existence of stellar populations with varied ages from young to old ages (Massey & Armandroff 1995; Sakai et al. 1999; Borissova et al. 2000; Sanna et al. 2008, 2009), including also a number of PNe and carbon stars, tracers of old/intermediate-age stellar populations (Magrini et al. 2003; Demers et al. 2004). However, with the exception of the most recent star formation, very little is known about

⋆ Based on observations obtained at the Gemini Observatory, which is operated by the Association of Universities for Research in Astronomy, Inc., under a cooperative agreement with the NSF on behalf of the Gemini partnership.

† E-mail: laura@arcetri.astro.it

the star formation history of IC10 (but see the recent results by Sanna et al. (2009)) or its age-metallicity relation.

In this framework, the aim of the present paper is to study spectroscopically two stellar populations of IC10: young stars through the emission-line spectra of the H II regions; and intermediate-age stars through PNe. The goal of this study is to reconstruct the star formation history of IC10 from the birth of the PN progenitors to very recent times, and to set up its age-metallicity relation.

This is possible thanks to the characteristics of the chemical abundances derived from PN and H II region spectroscopy. The progenitor stars of PNe, the low- and intermediate-mass stars (LIMS) $1M_{\odot} < M < 8M_{\odot}$, do not modify the composition of O, Ne (these two elements in a first approximation), S, and Ar in the material ejected during and after the Asymptotic Giant Branch (AGB) phase. Thus the PN abundances of these elements are characteristic of the composition of the ISM at the epoch when the PN progenitor was formed. On the other hand, He, N, C are modified in the ejecta, because processed during the lifetime of the progenitor stars. They hence give information on the stellar evolution of these stars. At the same time, the chemical abundances of H II regions are representative of the current composition of the interstellar medium (ISM). The analysis performed in this paper will be the starting point of a further work aiming at a complete understanding of the history of IC10 through the building of an 'ad hoc' chemical evolution model based on PN and H II region constraints (Lanfranchi et al., in prep.).

The paper is structured as follows: in § 2 we present the imaging observations used for mask design, while in § 3 we describe our spectroscopic observations with GMOS. In § 4 we introduce the determination of the physical and chemical properties of the nebulae, discuss the nebular abundance patterns together with the age dating of the PN progenitors. In § 5 we analyze the star formation history of IC10, whereas in § 6 we study the spatial metallicity distribution. Finally, in § 7 we approach the occurrence of the 3-rd dredge-up in PNe belonging to several dwarf irregular galaxies. In § 8 we present our summary and conclusions.

2 PRE-IMAGING

GMOS-N pre-imaging exposures were taken in order to identify the H II regions and PNe selected to build the mask for our multi-object spectroscopy, on August 08, 2007. The central region of IC10, within a field of view of $5.5' \times 5.5'$, was observed through two filters: the Hα one, HaG0310, with central λ 655 nm and width $\sim$7 nm and the Hα-continuum filter, HaCG0311, whose central λ is located in the continuum adjacent to Hα (λ_c 662 nm, width $\sim$7 nm). The exposure times were 400 s for each filter, split in two sub-exposures. The two narrow-band frames were used to build a Hα continuum-subtracted image, where we re-identified a large number of small and giant known H II regions, and three candidate PNe discovered by Magrini et al. (2003). In addition, a large number of new PN candidates (12) were discovered.

The criteria adopted to distinguish PNe from compact HII regions are similar to those employed by Peña, Stasińska & Richer (2007). In particular their criteria a), b), and d) are useful when only imaging observations are available, while e) is useful for spectroscopy. Their criterium c) is not applicable in our case. These criteria can be summarized in our case as the following:

1) at the distance of IC10 ($\sim$0.7-0.8 Mpc), $1''$ corresponds to about 3.6 pc. Given the FWHM of about $0.6''$ for point-like objects, PNe (which have typically diameters smaller than 1 pc) are expected to be unresolved. Thus *our candidate PNe were selected among point-like Hα-emitting objects*;
2) the central stars ionizing PNe are usually hotter than those ionizing H II regions (e.g. Stasińska 1990, Méndez, Kudritzki, & Herrero 1992). Due to their spectral type, with the energy maximum in the UV, PN central stars have lower M_V than the ionizing stars of H II regions (typically more than 2 mag fainter). Thus *we do not expect to detect PN candidates in the image taken with HaCG0311, whose central λ is located in the continuum adjacent to Hα.*
3) Due to multiple ionizing sources in H II regions, optically thick compact H II regions are expected to be brighter than optically thick PNe in the hydrogen recombination lines. Thus *our PN candidates are usually fainter in the Hα-continuum image than compact H II regions.*
4) From a spectroscopic point of view, the presence of HeII 4686 emission whose intensity exceeds a few percent of Hβ and/or intensity ratios [O III] 5007/Hβ larger than about 4 are found only in PNe. On the other hand, low-excitation PNe cannot be distinguished from H II regions only on the basis of their spectroscopic line ratios.

Our further spectroscopic study confirmed 9 of these 12 objects as true PNe– by the absence of continuum spectrum and/or from the high [O III] 5007/Hβ ratio (ranging from $\sim$4 to 16, with the exception of PN23, with a lower ratio). Among the point-like emission-line sources, we also revealed a symbiotic system (IC10-SySt-01), confirmed spectroscopically. Its analysis has been presented in a recent paper by Gonçalves et al. (2008). The remaining two candidate PNe were not included in the follow-up spectroscopy due to the intrinsic limits of the mask design.

We used the standard star BD+254 to calibrate the Hα image. We compared the photometry of PN05, PN07, PN09 with that by Magrini et al. (2003), finding an agreement with our measurements within $\sim$30%. The differences in the flux measurements are attributed to the non-photometric conditions of the observations in the present work.

The identification numbers, equatorial coordinates at J2000.0 and Hα+[N II] fluxes of the observed PNe and H II regions are shown in Table 1. ID numbers in Table 1 were assigned starting from the last number of the previous list of PN candidates in IC10 (ending with PN16; Magrini et al. 2003). Errors on the fluxes were computed taking into account the uncertainties in the photon statistics, the background, and the flux calibration. The PNe from 17 to 25 were spectroscopically confirmed, whereas the spectra of PN 26 and 27 were not observed.

3 SPECTROSCOPY

Spectra of IC10 PNe and H II regions were obtained in queue mode with GMOS-N, using two different gratings:

Table 1. Identification and photometry of the Hα emitters. *Top*: known PNe. *Middle*: new PNe candidates. *Bottom*: known H II regions.

ID	RA J2000.0	Dec	Hα+[N II][a]
IC10PN5	00:20:17.280	+59:15:53.39	1.68±0.20
IC10PN7	00:20:22.232	+59:20:02.57	110±0.50
IC10PN9	00:20:32.113	+59:16:02.45	3.51±0.21
PN17	00:19:57.487	+59:17:12.77	3.22±0.24
PN18	00:19:59.418	+59:19:03.53	0.64±0.16
PN19	00:20:03.103	+59:19:20.53	0.83±0.15
PN20	00:20:03.896	+59:19:27.41	2.76±0.19
PN21	00:20:14.798	+59:18:08.96	3.15±0.25
PN22	00:20:19.712	+59:18:13.81	3.97±0.27
PN23	00:20:23.695	+59:19:51.99	0.72±0.19
PN24	00:20:29.507	+59:16:41.38	3.72±0.29
PN25	00:20:33.235	+59:16:15.00	1.19±0.15
PN26	00:20:05.721	+59:18:11.99	1.14±0.15
PN27	00:20:34.002	+59:18:15.00	2.23±0.16
IC10-SySt-01	00:20:33.593	+59:18:46.86	1.36±0.16
HL90 13	00:20:04.270	+59:16:56.53	-
HL90 20	00:20:10.025	+59:19:14.92	-
HL90 29	00:20:12.864	+59:20:09.05	102.3[b]
HL90 30	00:20:13.299	+59:20:13.36	109.6 [b]
HL90 40	00:20:16.719	+59:20:28.92	9.55[b]
HL90 45	00:20:17.439	+59:18:40.14	1230.3[b]
HL90 50	00:20:19.256	+59:18:55.30	794.3[b]
HL90 51	00:20:19.370	+59:18:03.42	19.05[b]
HL90 107	00:20:25.921	+59:16:49.71	57.5[b]
HL90 111	00:20:27.584	+59:17:25.643	2818.4[b]
HL90 120	00:20:27.633	+59:17:37.70	38.9[b]
HL90 122	00:20:27.887	+59:18:21.28	42.6[b]
HL90 127	00:20:29.396	+59:17:55.30	7.94[b]
HL90 141	00:20:32.462	+59:17:50.337	38.0[b]

[a] $\times 10^{-16}$ erg cm^{-2} s^{-1}.
[b] Fluxes from Hodge & Lee (1990).

R400+G5305 ('red'), with 3 exposures of 1,700s each, on October 11, 2007; and B600+G5303 ('blue') with 4×1,700s exposures, on October 14 and 18, 2007. The slit width was 1″, while their heights varied from 5″ to 10″ for PNe, and from 5″ to 30″ for H II regions. Each exposure was offset by ± 3″ from one another (positions A: -3″,B: 0″, C: +3″, and D as A, for B600). The pixel binning were 2×2 (spectral×spatial). The spatial scale and reciprocal dispersions of the spectra were as follows: 0.″094 and 0.3 nm per binned pixel, in 'blue'; and 0.″134 and 0.8 nm per binned pixel, in 'red'. Seeing varied from ∼0.5″ to ∼0.6″ for the R400 spectra, and it was ∼0.6″ for the two runs in which B600 spectra were taken. CuAr lamp exposures were obtained with both gratings for wavelength calibration. The effective 'blue' plus 'red' spectral coverage was generally from 3700 Å to 9100 Å. Due to the slit location some spectra have a different spectral range (starting up to 300Å above the lower limit, with the same $\Delta\lambda$, for instance, from ∼4000 Å to 9400 Å).

Data were reduced and calibrated using the Gemini GMOS DATA REDUCTION SCRIPT and LONGSLIT tasks, both being part of IRAF[1]. The sky- and background-subtraction task deserves a particular explanation, due to the difficulty of performing it in the central regions of IC10. The usual method consists in the definition, for each slit, of the object extension and one small (few arcsec) extension of the sky. In the central regions of the galaxy this was not possible since the slit was totally occupied by the emission-line source. Thus we allocated several slits in the external part of IC10, where no diffuse emission was present, to serve as sky template. We used them when the slit was completely filled by the source.

The other method of sky- and background-subtraction takes advantage of three exposures in the 'red' and four in the 'blue' spectroscopic frames. In fact, the exposures were offset by ± 3″ from one another (positions A: -3″,B: 0″, C: +3″, and D as A, but only for the blue part). As the sky transparency vary between the different exposures, we allowed a factor of normalization adjusted in order to best remove the sky emission lines. The subtraction was performed taking into account the difference spectra: A-B, A-C, and B-C. The final spectra were the average of the three individual pairs (A-B, A-C, and B-C) of sky-subtracted objects. Note that the extraction of all H II regions has been limited to the bright central 2-3″region for obvious reasons. The second method gives much better results in the sky-subtraction, especially in the near IR part of the spectra, and therefore was the method used when possible, especially for PNe.

Spectra of the spectrophotometric standard Wolf1346 (Massey et al. 1988; Massey & Gronwall 1990), obtained with the same instrumental setups as on September 17 and October 5, 2007, were used to calibrate the spectra. This allowed to recover the actual slope of the spectrum, although not its flux zero point. This is not essential for our aims, for which only a relative calibration in flux is necessary.

The emission-line fluxes were measured with the package SPLOT of IRAF. Errors on the fluxes were calculated taking into account the statistical errors in the measurement of the fluxes, as well as systematic errors of the flux calibrations, background determination, and sky subtraction.

The observed line fluxes were corrected for the effect of the interstellar extinction using the extinction law of Mathis (1990) with R_V=3.1. We used c_β as a measurement of the extinction, which is defined as the logarithmic difference between the observed and theoretical Hβ fluxes. Since Hδ and Hγ are only available in few cases and are affected by larger uncertainties, c_β was determined comparing the observed Balmer I(Hα)/I(Hβ) ratio with its theoretical value, 2.85 (Osterbrock & Ferland 2006).

Tables A.1 and A.2, in the Appendix section, give the results of the emission-line flux measurements and extinction corrected intensities for PNe and H II regions, respectively.

The emission-line measurements of PN18 and PN19 are not presented in Table A.1. On one side, PN18 had its Hβ emission line unmeasured because it fell within a CCD gap. In addition, PN18 is a faint object and the only emission lines measurable in its spectrum are; [O III] 5007, Hα, and the [N II] and [S II] doublets. On the other side, for the extremely faint PN19 we could measure only the [O III] 5007Å

[1] IRAF is distributed by the National Optical Astronomy Observatory, which is operated by the Association of Universities for Research in Astronomy (AURA) under cooperative agreement with the National Science Foundation.

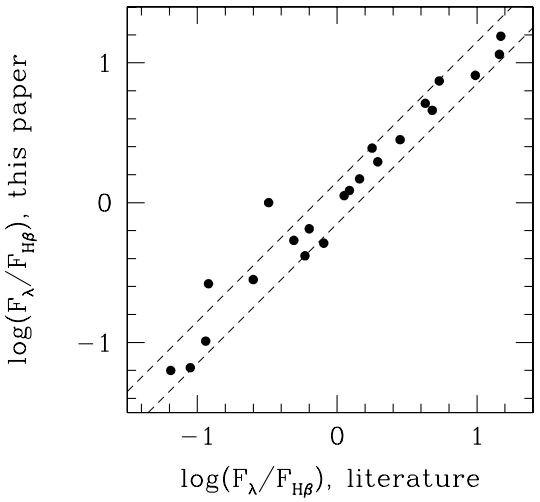

Figure 1. Comparison of the observed flux measurements of the present work with previous spectroscopic studies of the emission-line population of IC10 (H II regions: Lequeux et al. 1979 and Richer et al. 2001; PNe: Kniazev et al. 2008).

and Hα lines. Instead of appearing in Table A.1, the emission line measurements of IC10PN7 –which turned to be an extended H II region composed by two knots, as already pointed out by Kniazev et al. (2008)– are presented in Table A.2.

We compared the observed emission line fluxes of Tables A.1 and Tables A.2 with those emission line fluxes in common with previous studies (H II regions: Lequeux et al. 1979 and Richer et al. 2001; PNe: Kniazev et al. 2008). A good agreement is found not only for the bright emission lines of H II regions and PNe, but also for the faintest cases, proving the reliability of the spectroscopy discussed here (see Figure 1).

4 PHYSICS AND CHEMISTRY OF THE NEBULAE

4.1 Determination of nebular physical and chemical properties

The extinction-corrected intensities were used to obtain the electron densities and temperatures of each nebula, PN or H II region. To calculate the densities we used the doublet of the sulfur lines [S II]$\lambda\lambda$6716,6731, while for the electron temperatures we used the ratios [O III]λ4363/(λ5007+λ4959) and [O III]λ3727/(λ7320+λ7330) and in few cases [N II]λ5755/(λ6548+λ6584) and [S III]λ6312/(λ9059 + λ9512). The [N II] and [O II] line ratio gives the low-excitation temperatures, while the [O III] and [S III] line ratios give the medium-excitation temperatures (see also Osterbrock & Ferland 2006, §5.2). Plasma diagnostics were calculated using the 5-level atom model included in the NEBULAR analysis package in IRAF/STSDAS (Shaw & Dufour 1994). The [O III] λ4363 emission line was measurable with a sufficiently high signal to noise ratio in 4 H II regions and 1 PN, while an upper limit to the [O III] λ4363 could be given for 6 H II regions and 5 PNe. Due to the lower excitation of H II regions respect to PNe we could derive T_e[OII] in 6 of them. We also could directly derive T_e[NII] in HL90 45 and T_e[SIII] in HL90 51.

The temperature and density uncertainties have been estimated by formal error propagation of the absolute errors on the extinction-corrected line fluxes. Typical errors on electron temperatures and densities are shown in Table 2 for nebulae with at least one electron temperature measured. For the remaining objects, electron temperatures are given in Table 3 and 4 as upper limits.

Ionic abundances were computed using the NEBULAR analysis package. Elemental abundances were then determined by applying the ionization correction factors (ICFs) following the prescriptions by Kingsburgh & Barlow (1994) for the case where only optical lines are available.

For the abundance analysis we used, when available, T_e[OII] and T_e[NII] for the calculation of the N^+, O^+, S^+ abundances, while T_e[OIII] was used for the abundances of O^{2+}, S^{2+}, Ar^{2+}, He^+, and He^{2+}. In the remaining objects, where only T_e[OIII] was measured, we adopted it both for low- and high-ionization species. The abundances of HeI and HeII were computed using the equations of Benjamin, Skillman & Smits (1999) in two density regimes, i.e. N_e >1000 cm^{-3} and $\leqslant$1000 cm^{-3}. The Clegg's collisional populations were taken into account (Clegg 1987).

The remaining PNe and H II regions, those for which no estimations of electron temperature could be given, are not reliable for any calculation of chemical abundances.

In Table 2 we present the typical errors on the total chemical abundances for nebulae with at least one direct estimate of electron temperature. In this table H II regions and PNe are grouped in bins that correspond to their observed Hα flux in Table 1. Errors on electron temperatures and densities are given in percentage, while errors on He/H are absolute and given on the quantity expressed by number. Finally, errors on the total metal abundances are in dex on the quantities expressed in the usual 12+log(X/H) form.

In Tables 3 and 4 we present electron temperatures and densities, ionic abundances, ionization correction factors, and total abundances, for PNe and H II regions, respectively. In these tables, the quantities derived using an upper limit determination of the electron temperature are marked with '>' for the forbidden lines and '<' for the recombination lines, according to their dependence on T_e.

4.2 Abundance patterns: PNe and H II regions

We compared the abundance ratio of PNe and H II regions of IC10 with the relations derived by Izotov et al. (2006) from observations of a large sample of blue-compact galaxies, BCGs. These relations are marked by continuous lines in Figure 2, while their 1-σ dispersion is indicated by two dashed lines. In the Izotov et al.'s sample, the α element-to-oxygen abundance ratios Ne/O, S/O and Ar/O do not show large trends with oxygen abundance, due to their common origin. The best determined ratio, Ne/O, increases slightly with increasing O/H (by $\sim$0.1 dex in the analyzed range). This can be explained by the depletion of oxygen onto dust grains with $\sim$20% of oxygen locked in dust. Due to the large dispersion of N/O and the different stellar origin of nitrogen

Table 2. Typical errors for nebulae with measured electron temperature. *a)* Errors on electron temperatures and densities are given in percentage, *b)* errors on He/H are absolute and given on the quantity expressed by number, while *c)* errors on the total metal abundances are in dex on the quantities expressed in the usual 12+log(X/H) form.

Hα flux 10^{-15} erg/cm^2 s	n_e^a %	T_e[OII]^a %	T_e[OIII]^a %	Δ(He/H)^b number	Δ(O/H)^c dex	Δ(N/H)^c dex	Δ(Ne/H)^c dex	Δ(Ar/H)^c dex	Δ(S/H)^c dex	N(PNe)	N(H II)
1-10	-	-	12%	0.03	0.10	0.15	-	-	0.40	1	-
10-50	25%	9%	12%	0.008	0.08	0.30	0.40	0.20	0.50	-	2
50-100	20%	-	10%	0.007	0.07	-	-	-	-	-	1
100-1000	15%	7%	5%	0.005	0.06	0.15	0.30	0.15	0.40	-	4
>1000	10%	5%	5%	0.002	0.05	0.15	0.15	0.10	0.30	-	2

Table 3. Physical and chemical parameters of the PN sample. < and > symbols mark the limits (upper or lower) on the total and ionic chemical abundance derived with upper limit (<) determinations of the electron temperature.

Id	IC10PN5	IC10PN9	PN17	PN20	PN21	PN22
Te(OIII)	<13000	<11000	14100	<10800	<15000	<14700
Ne(SII)	300	8500	-	3200	3100	4400
HeI/H	<0.137	<0.111	0.147	<0.086	<0.101	<0.060
HeII/H	<0.01	<0.003	0.009	-	<0.007	<0.013
He/H	<0.149	<0.115	0.138	<0.086	<0.108	<0.072
OII/H	-	>5.67e-05	3.04e-05	-	-	>9.03e-05
OIII/H	>1.78e-04	>3.29e-04	5.83e-05	>2.98e-04	>4.14e-05	>1.37e-04
ICF(O)	1.05	1.02	1.02	1.00	1.01	1.02
O/H	>1.88e-04	>3.93e-04	9.19e-05	>2.98e-04	>4.19e-05	>2.33e-04
12+log(O/H)	>8.27	>8.59	7.96	>8.47	>7.62	>8.37
NII/H	>3.35e-06	>5.36e-06	3.68e-06	-	-	>4.51e-06
ICF(N)	-	6.94	3.00	-	-	2.58
N/H	-	>3.72e-05	1.11e-05	-	-	>1.16e-05
12+log(N/H)	-	>7.57	7.05	-	-	>7.06
ArIII/H	>5.46e-07	>7.12e-07	-	>1.00e-06	>5.32e-07	>6.59e-07
ICF(Ar)	1.87	1.17	-	1.87	1.87	1.635
Ar/H	>1.02e-06	>1.33e-06	-	>1.87e-06	>9.95e-07	>1.23e-06
12+log(Ar/H)	6.00:	>6.12	-	>6.27	>6.00	>6.09
SII/H	>8.69e-08	>2.46e-07	7.74e-8	>6.33e-07	>5.17e-07	>1.32e-07
SIII/H	>5.40e-07	-	2.38e-06	>6.77e-07	>1.41e-06	>8.58e-07
ICF(S)	-	1.39	1.05	-	-	1.09
S/H	-	>2.68e-06	2.49e-06	-	-	>1.08e-06
12+log(S/H)	-	>6.43	6.40	-	-	>6.03

and oxygen, Izotov et al. (2006) do not present a relation of this ratio with 12+log(O/H) (see, e. g., Figure 11 of Izotov et al. 2006 and the large scatter for 12+log(O/H)>8).

The abundance ratios of IC10 H II regions are generally in good agreement with the trends of BCGs. The Ne/O ratio is measured in 4 H II regions and shows little dispersion: Ne/O=0.13±0.04, which means log(Ne/O)=-0.89±0.10dex. It is slightly lower than the value found by Izotov et al. (2006), but still consistent with their relation.

The values of log(N/O) in the H II region sample show a larger dispersion (-1.0 ± 0.3) than Ne/O, but they are consistent with the values assumed by BCGs in the same metallicity range (see Figure 11 of Izotov et al. 2006, where for 12+log(O/H)=8.3, the corresponding log(N/O) ranges from approximately -1.3 to -0.9). However, considering the recent star formation history of IC10, which is having a strong starburst, we would expect to measure a lower value of N/O. In fact, in the delayed-release hypothesis, i.e. the moderate-time-delayed production of nitrogen by intermediate mass stars (Pilyugin, Thuan, & Vílchez 2003), N/O would drop while O/H increases as massive stars begin to die and eject oxygen into the interstellar medium. At the point when all the massive stars have died, the N/O value would be at its minimum. The reason why the N/O value in IC10 is consistent with other BCGs has to be searched in the fact that anything ejected by massive stars –whether oxygen by type II supernovae or nitrogen in the winds of WR stars–, will not be immediately incorporated into the nebular gas. In fact, this ejected matter is too hot, and needs to cool before it can mix with the ISM and be seen in the optical spectra of nebular gas. In addition, we note that there is a single H II region with a higher N/O value, namely HL90-120. We thus consider for this region, which contains four known W-R stars within 20″ from its center, a possible zone of nitrogen pollution. A large presence of Wolf-Rayet stars could, indeed, produce isolated regions with enhanced nitrogen (López-Sánchez & Esteban 2008).

For the three PNe for which we measured the N/O ratio, we obtain values close to those expected for the H II regions in BCGs. From the nucleosynthesis of the PN progenitors, one would expect an enhancement of the N/O ratio since PNe commonly synthesize and dredge-up nitrogen. Recently, Richer & McCall (2007) have shown that, often, the brightest PNe in star-forming galaxies have N/O ratios very similar to those in the H II regions. The values of both Ar/O and S/O of H II regions and PNe are in agreement with the Izotov et al.'s (2006) relations. The decreasing trend of Ar/O vs. O/H might be due to the adopted ICF for Ar.

Table 4. Physical and chemical parameters of the H II region sample. < and > symbols mark the limits (upper or lower) on the total and ionic chemical abundance derived with upper limit (<) determinations of the electron temperature.

Id	IC10PN7	HL90 20	HL90 29	HL90 30	HL90 45	HL90 51	HL90 50	HL90 107	HL90 111	HL90 120
Te(OIII)	<10600	<11000	14100	<13500	10100	<11600	12300	<12350	<10200	10300
Te(OII)	9500	8300	7500	-	-	-	8600	-	9700	15000
Te(NII)	-	-	-	-	11600	-	-	-	-	-
Te(SIII)	-	-	-	-	-	-	9200	-	-	-
Ne(SII)	180	-	-	700	530	600	150	650	-	613
HeI/H	0.091	0.099	0.132	<0.105	0.102	<0.080	0.121	<0.091	0.086	0.054
OI/H	3.24e-06	-	-	-	1.25e-04	>1.67e-06	1.46e-06	>4.02e-06	-	5.26e-07
OII/H	4.92e-05	9.44e-05	3.994e-04	>1.06e-05	2.300e-05	>2.24e-05	8.77e-05	>1.54e-05	6.218e-05	4.381e-06
OIII/H	1.16e-04	8.702e-05	8.89e-05	>4.44e-05	2.613e-04	>8.94e-05	6.6e-05	>1.40e-04	6.249e-05	1.38e-04
O/H	1.69e-04	1.82e-04	4.88e-04	>5.53e-05	2.87e-04	>1.14e-04	1.56e-04	>1.61e-04	1.264e-04	1.53e-04
12+log(O/H)	8.23	8.26	8.68	>7.74	8.45	>8.05	8.19	>8.21	8.10	8.18
NII/H	5.44e-06	5.675e-06	2.00e-05	>2.44e-05	1.315e-06	>3.0e-05	4.950e-06	>2.39e-06	5.858e-06	1.44e-06
ICF(N)	3.43	1.92	1.22	5.2	12.5	1.55	5.08	10.5	2.032	34.9
N/H	1.87e-05	1.09e-05	2.45e-05	>1.2e-05	1.64e-05	>1.53e-04	8.8e-06	>2.51e-05	1.191e-05	5.04e-05
12+log(N/H)	7.27	7.03	7.40	>8.10	7.21	>8.18	6.95	>7.40	7.08	7.70
NeIII/H	1.01e-05	-	-	-	4.69e-05	-	9.26e-06	-	-	1.52e-05
ICF(Ne)	1.46	-	-	-	1.09	-	2.36	-	-	1.10
Ne/H	1.47e-05	-	-	-	5.14e-05	-	2.18e-05	-	-	1.68e-05
12+log(Ne/H)	7.17	-	-	-	7.71	-	7.34	-	-	7.22
ArIII/H	9.23e-07	0.87e-06	0.86e-06	>0.57e-06	1.13e-06	>8.00e-07	7.45e-06	> 0.950e-06	1.100e-06	0.62e-06
ICF(Ar)	1.41	2.1	5.5	1.23	1.08	1.24	2.28	1.10	1.969	1.03
Ar/H	1.73e-06	1.58e-06	1.60e-06	>1.06e-06	2.13e-06	>1.49e-06	1.39e-06	>1.78e-06	2.057e-06	1.23e-06
12+log(Ar/H)	6.24	6.20	6.20	>6.03	6.32	>6.17	6.14	>6.25	6.31	6.10
SII/H	4.34e-07	6.80e-07	3.65e-06	>3.12e-07	2.31e-07	>4.26e-07	6.221e-07	>0.69e-06	7.446e-07	1.67e-07
SIII/H	3.690e-07	2.13e-06	1.90e-06	>2.090e-06	1.74e-06	>2.76e-06	3.46e-06	>5.06e-06	-	1.52e-06
ICF(S)	1.26	1.04	1.010	1.28	1.65	1.27	1.029	1.57	1.048	2.28
S/H	4.08e-06	2.92e-06	2.26e-06	>3.02e-06	3.27e-06	>4.07e-06	4.20e-06	>9.03e-06	5.212e-06	3.88e-06
12+log(S/H)	6.67	6.46	7.35	>6.48	6.51	>6.61	6.62	>6.95	6.72	6.59

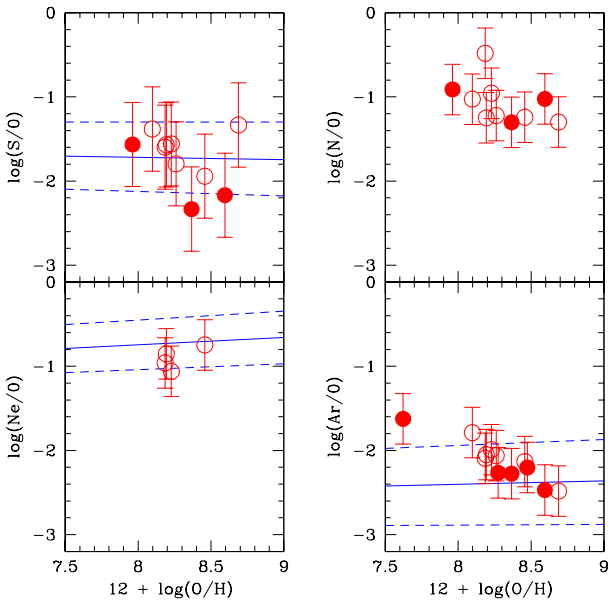

Figure 2. Chemical abundance patterns for PNe (filled circles) and H II regions (empty circles), compared with the relations of Izotov et al. (2006) for the α-element to oxygen ratios. The Izotov's relations are marked with continuous lines, while their dispersion is indicated with dashed lines.

4.3 The nature of the PN population: dating the progenitors

The abundance ratios N/O and He/H are useful to discriminate PNe of different types, which means PNe deriving from progenitors with different initial mass and thus formed in different epochs. The N/O ratio provides information about the stellar nucleosynthesis during the AGB phase of LIMS. In fact, nitrogen is produced in AGB stars in two ways: by neutron capture, during the CNO cycle; and by hot-bottom burning. Hot-bottom burning produces primarily nitrogen but occurs only if the base of the convective envelope of the AGB stars is hot enough to favor the conversion of ^{12}C into ^{14}N. Thus nitrogen is expected to be mostly enriched in those PNe with the most massive progenitors, i.e. with turnoff mass larger than $\sim$3 M$_\odot$ (van den Hoek & Groenewegen 1997; Marigo 2001). The He/H abundance gives also an indication of the initial mass of the progenitor: the nebula is enriched progressively for more massive stars; it reaches a plateau between 3 and 4 M$_\odot$; and then it increases again toward the higher masses (Marigo 2001). However, He/H is a weaker indicator of the PN types in low metallicity environments.

Since the oxygen abundance of IC10 is very similar to those of the LMC and of the M33, we can use the Type I limits as in Dopita (1991) and Magrini et al. (2009): Type I PNe are those with log(N/O)>-0.5 independently of the helium abundance. From Table 3 we see that N/H is available for three PNe, namely IC10-PN9, PN17, and PN22. Following the definition by Dopita (1991) these PNe are non-Type I. For the remaining PN we have not a sure determination of their type. Since the N/O ratio is low for all three PNe, high mass progenitor stars can be ruled out for them. Therefore, their progenitor stars are of mass, M <1.2 M$_\odot$, and consequently they were born during the first half of the age of the Universe.

For the PNe without any determination of the N/O ratio, another aspect of their spectra points out that they

have old progenitors. The HeII intensities are all very low or not detectable, which implies that the central stars are on the horizontal portion of their evolutionary tracks. This can happen irrespective of the age/mass of the progenitor stars, but it is more likely if the stars are of low mass since the PNe will have lower mass central stars that evolve to high temperature more slowly.

4.4 The chemical evolution of IC10 and comparison with other galaxies

In Table 5 we compare the average chemical abundance of the PN and H II region populations of IC10 with those of SMC, LMC, M33, and the Milky Way galaxies. The uncertainties given in Table 5 are the standard deviations of the average values, computed by number and then converted in the logarithmic form. The large *rms* uncertainties both in PN and H II region average abundances are due to their spatial variations through the disk of IC10.

First of all, by comparing the average abundances of the α-elements of the PNe of IC10 with those of its H II regions, we found that they nearly match, with the PN abundances slightly lower. In particular, S/H and Ar/H are lower in PNe than in H II regions, while O/H is unchanged, within the errors. Note that oxygen is the best measured element and at the metallicity of IC10 it is not modified during the lifetime of LIMS (see the detailed discussion in §7). Thus, we can adopt it as a tracer of the past ISM metallicity. At a first look the enrichment history of IC10 can be thus estimated by comparing the average O/H of H II regions, e.g. the present-time ISM, to the O/H of PNe, the ISM at the epoch of the birth of the progenitor LIMS. From this comparison, we found a small variation in the average metal content of IC10, from the epoch of the formation of the PN progenitors (see Sect. 4.3) to the present time. However, we remind that only a single PN has a direct measurement of the electron temperature. The average PN abundance in Table 5, marked with *a*, also includes upper limit electron temperatures, i.e., lower limit oxygen abundances. Unfortunately, no abundance determination from other stellar populations than H II regions are available in the literature. Previous chemical abundances were based on spectroscopic observations of H II regions by Lequeux et al. (1979), then recomputed with updated atomic data and ICF by Skillman et al. (1989) and Garnett (1990), and more recently by new spectroscopic observations of Richer et al. (2001). These abundance determinations are in good agreement with ours, but do not extend the temporal range. The reasons for the little change in the global metallicity of IC10 have to be searched in the strong winds and outflows that are affecting its chemical evolution. These winds are believed to be strongly differential and to allow mainly the lost of α-elements expelled through Type II supernova winds (e.g, Mac Low & Ferrara 1999, Recchi et al. 2008).

Secondly, let's compare the chemical abundances of PNe in different galaxies: the metallicity of the PNe in IC10 is sub-solar, and their average oxygen abundance is very close to those of the LMC and M33. While a good agreement is noticed among PNe α-element abundances, both N/H and consequently N/O are lower than the corresponding values in LMC and M33.

Finally, by examining the H II regions we find again a good agreement with M33, with N/O ratio consistent with the average value of M33's H II regions. Thus, it seems that the main difference between the average abundances (PN and H II regions) of IC10 and M33 is in the behaviour of the N/O ratio: while N/O is similar in the H II regions of both galaxies, it results to be higher in M33 PNe than in IC10 PNe. Is this a signature of different past star formation histories or a lack of nitrogen enrichment in the PN progenitors? Probably the presence of a number of Type I PNe in M33, which are indeed absent in IC10, enhance the N/O average value. As in other dIrrs, many of the progenitors of PNe do not show evidence of nitrogen dredge-up, which might be a uncommon process in such low metallicity environments. An interesting discussion on the N/O and the nucleosynthesis processes in the progenitors of PNe in dIrr galaxies is treated by Richer & McCall (2007). Considering a sample of bright PNe (i.e., within 2 mag from the bright cutoff of their luminosity function) in several nearby dIrrs they found that PNe have oxygen abundances close to the ISM values and also N/O has little variations in the two populations. Since the Ne/O ratio is in agreement with the ISM one, they conclude that nor oxygen neither neon are modified during the PNe lifetime. Thus, since O/H is close the H II regions' one, they conclude that these PNe arise preferentially as a result of a recent star formation. But in IC10, this conclusion is difficult to reconcile with the estimated large age of PNe, both from their low HeII lines and their low N/O ratio, which are both hints of low mass (thus old) progenitors. In IC10, the characteristics of PNe are more consistent with an old/intermediate-age population formed from an ISM which had a small or null enrichment during the second half of the Universe lifetime. In this scenario, their low mass (see §4.3) is in agreement with no nitrogen dredge-up, and thus low N/O.

5 THE STAR FORMATION HISTORY OF IC10

The spectroscopically observed PNe, all with low N/O ratio and/or with very low or absent HeII, are, in a first approximation, 'old stars', thus they could be born in a limited period of time, 7 to 11 Gyr ago, i.e., during the first half of the age of the Universe. Following the discussion of Magrini et al. (2005b), we obtain that the mass of the stellar population born during the epoch of the PN progenitors' formation, is proportional to the number of PNe. About $2\times10^6 M_\odot$ were formed by each observed PN.

Thus, we considered the two surveys for PNe in IC10: the present one and that by Magrini et al. (2003). The current survey is the deeper one, since it discovered 12 PNe in an area of $5.5'\times5.5'$, where the previous survey found only three. The previous study surveyed an area of $33'\times33'$ and lead to the discovery of 15 candidate PNe. If the survey by Magrini et al. (2003) reached the same depth as the present search, this would imply the presence of about 60 (i.e., four times the previous number of known PNe). Thus the mass of the underlying population would be approximately $1.2\times10^8 M_\odot$. This corresponds to a star formation rate (SFR) of about 0.02 $M_\odot$ yr^{-1} if the star formation bursts were extended through a long period of about 7 Gyr. If we consider that all PNe belong to the same age range, 7-10 Gyr old, thus the SFR would be 0.04 $M_\odot$ yr^{-1}. This

Table 5. Average chemical abundances and abundance ratios of PN and H II region samples in several galaxies. The first column indicates the sample; columns from 2 to 7 show the average elemental abundances expressed by number; columns 8 and 9 give the mean values of N/O and Ne/O. *a)* Chemical abundances computed also including upper limit electron temperature determinations; *b)* chemical abundances computed using only direct electron temperature determinations; *c)* Stanghellini (2008); *d)*; Magrini et al. (2009) *e)* Stanghellini et al. (2006); *f)* Asplund, Grevesse & Sauval (2005).

Sample	He/H	O/H ($\times10^{-4}$)	N/H ($\times10^{-4}$)	Ne/H ($\times10^{-5}$)	Ar/H ($\times10^{-6}$)	S/H ($\times10^{-6}$)	N/O	Ne/O
IC10 PNe[a]	0.107±0.032	2.07±1.30	0.20±0.15	-	1.29±0.35	2.08±0.87	0.09±0.04	-
IC10 PN-17[b]	0.147±0.03	0.91±0.1	0.11±0.02	-	-	2.5±0.8	0.11±0.1	-
SMC PNe[c]	0.113±0.022	1.05±0.46	0.28±0.33	1.77±1.32	0.59±0.59	4.80±6.57	0.28±0.50	0.17 ±0.08
LMC PNe[c]	0.103±0.026	2.32±1.65	1.48±1.75	4.04±3.60	1.14±0.72	3.46±8.88	0.87±1.15	0.17 ±0.09
M33 PNe[d]	0.118±0.075	2.33±1.58	1.40±2.49	4.91±4.14	1.20±0.57	5.91±3.58	0.40±0.31	0.17±0.06
Galactic PNe[e]	0.123±0.042	3.53±1.95	2.44±3.46	9.68±7.98	1.26±1.24	-	0.67±0.82	0.25±0.10
IC10 HII regions[a]	0.107±0.031	2.31±1.59	0.38±0.39	2.62±1.76	2.49±2.81	7.45±6.62	0.10±0.10	0.13±0.04
IC10 HII regions[b]	0.100±0.024	2.23±1.28	0.20±0.14	2.62±1.71	1.67±2.81	6.68±7.10	0.11±0.10	0.13±0.04
M33 HII regions[d]	0.101±0.015	2.04±0.75	1.28±0.57	4.24±2.61	1.31 ±0.45	5.85±2.28	0.06±0.02	0.20±0.06
Solar value[f]	0.085±0.02	4.57±0.04	0.60±0.09	6.9±1.0	1.51±0.30	13.8±2.0	0.13±0.10	0.15±0.05

SFR is comparable to that found at present time using the observed Hα flux: 0.04-0.08 $M_\odot$ yr^{-1} (Thronson et al. 1990).

6 THE METAL DISTRIBUTION IN THE ISM OF IC10

Recent observations allowed a deeper knowledge of nearby dwarf galaxies, resolving the spatial distribution of their metal content. These results are giving indications of a non-homogeneous chemical composition also at large scales, as, for instance, in the dwarf irregular galaxies of the Local Group and nearby groups NGC 6822 (Lee et al. 2006), Sextans B (Kniazev et al. 2005, Magrini et al. 2005a), NGC 4214 (Drozdovsky et al. 2002, Kobulnick & Skillman 1996); and in the blue compact galaxies SBS0335-052 (Izotov et al. 2006) and Mrk86 (Gil de Paz, Zamorano & Gallego 2000).

Our and previous observations of IC10 show evidence of abundance non-homogeneities. The H II regions (and PNe) under analysis in this paper are located in the central 5.5′×5.5′, that, at the distance to IC10, means a projected area of 1.3×1.3 kpc. Typical angular distances between the H II regions of our sample are ∼1-1.5′, thus ∼300-400 kpc. The average abundance of oxygen in H II regions, considering only those where at least one electron temperature, T_e[OIII] and/or T_e[OII] was measured, is 2.2±1.3×10^{-4} by number, or 12+log(O/H)=8.30±0.20. The dispersion is comparable with those of other dwarf irregular galaxies whose metallicity map was recently obtained. For instance, the average oxygen abundances, are: 7.77 with a smaller dispersion of 0.07 dex for the H II regions of NGC 3109 (Peña et al. 2007), 7.6±0.2 for Sextans A, and 7.8±0.2 for Sextans B (Kniazev et al. 2005, Magrini et al. 2005a); and 8.06±0.09 for the SMC (see Peña et al. 2007).

Chemical abundance determinations of H II regions in IC10 were first derived by Lequeux et al. (1979) who observed its two brightest regions, named IC10-1 and IC10-2, which we re-identified as HL90-45 and HL90-111 (Hodge & Lee 1990). The study of Lequeux and collaborators indicated a notable difference in the chemical compositions of H II regions located in different areas of the galaxy: HL90-45 was found to have 12+log(O/H)=8.45 whereas for HL90-111 this abundance is 8.11, in good agreement with our results shown in Table 5. More recently, Richer et al. (2001) obtained chemical abundances of three IC10 H II regions: HL90-106b (with O/H 7.86±0.32), HL90-111c (7.84±0.25), HL90-111d (8.23±0.09). Again a notable difference in chemical composition is found and, in addition, a difference in the chemical composition within the same H II region complex, HL90-111, was derived: HL90-111c and Hl90-111d show that the variance of chemical abundances is in place also at small scales. The inhomogeneity revealed in HL90-111 is similar to that found in 30 Doradus by Tsamis & Péquignot (2005) for which they claimed the evidence for incomplete small-scale mixing of the ISM. In addition, very recent deep optical data collected by Sanna et al. (2009) suggest the presence of a spread in heavy element abundances of the order of one-half dex.

The O/H abundance vs. galactocentric radius is shown in Figure 3. Due to the uncertainties on the position angle and on the inclination of IC10, the galactocentric radius has been computed without any de-projection, thus considering that at a distance of 750 kpc, 1″ corresponds to 3.6 pc. Note that there is no indication of radial metallicity gradients, neither for H II regions nor for PNe.

The scale-length of metallicity non-homogeneities is of the order of 0.2-0.3 kpc, with clumps showing the higher metallicities, HL90-29 and HL90-45, and an area with a more constant metallicity, around 12+logO/H=8.2, located between 0.2 to 0.5 kpc from the center. For PNe the abundance determination are upper limits, with the exception of PN17, thus their metallicity map remains quite uncertain.

7 THE THIRD DREDGE-UP AND ITS EFFECT ON THE PN COMPOSITION

In contrast to H II regions, some elemental abundances in PNe are affected by the nucleosynthesis in the PN progenitors. Newly synthesized material can be dredged up by convection in the envelope, significantly altering the abundances

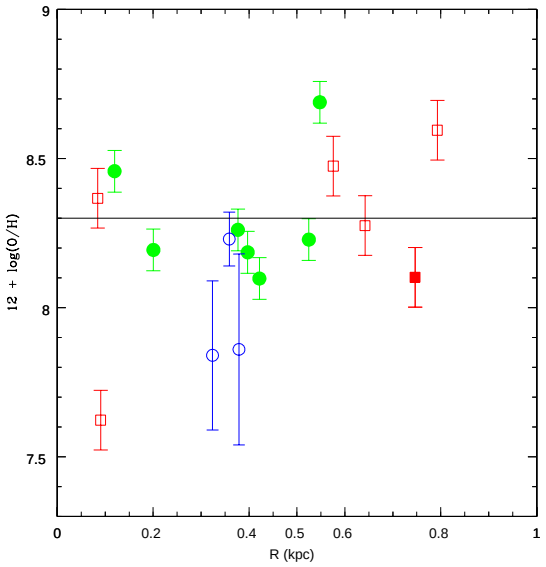

Figure 3. Oxygen abundance vs. galactocentric radius, not deprojected. Symbols represents data from: H II regions from the present paper, only those with T_e measured (filled circles); H II regions from Richer et al. (2001) (empty circles); PNe from the present work (filled square with T_e measured, empty square with upper limit of T_e). The continuous line represents the average O/H from our H II regions.

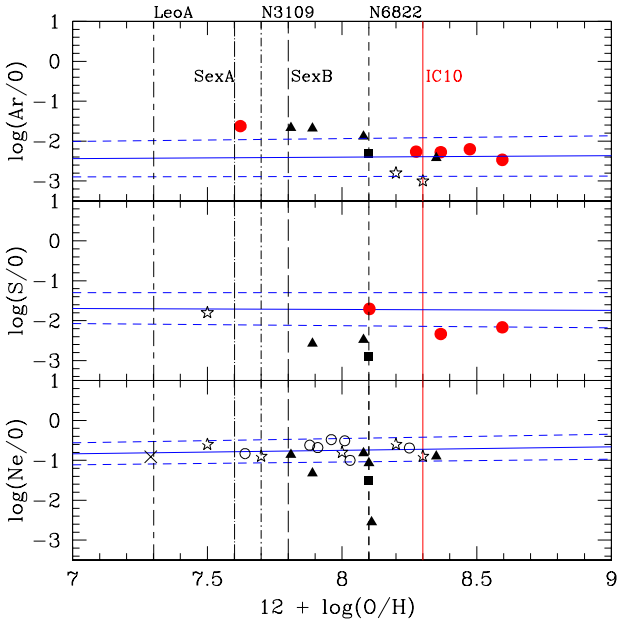

Figure 4. The planetary nebulae Ne/O, S/O and Ar/O abundance ratios as a function of the oxygen abundance of the PNe in a number of nearby dwarf irregular galaxies. Symbols for IC10 PNe are filled circles. For the other galaxies they are as follows: cross for Leo A; filled triangles for NGC 3109; filled square for Sex A; empty stars for Sex B; and empty circles for NGC 6822. The quasi-horizontal lines show the abundance line ratios given by the a sample H II regions of blue compact galaxies, as compiled by Izotov et al. (2006). The vertical lines show the 12+log(O/H) of the H II regions of each of the dIrr in this plot. These lines are labeled with the corresponding galaxy identification at the top of the plot.

of He, C and N in the surface layers during the evolution of the PN progenitor stars on the giant branch and asymptotic giant branch (AGB). Also a certain amount of oxygen can be mixed in during the thermally pulsing phase of the AGB evolution (Kingsburgh & Barlow 1994; Péquignot et al. 2000; Leisy & Dennefeld 2006).

However, the dredge-up of oxygen and neon seems a rare event, happening mainly in low metallicity environments. This has induced us to believe that oxygen is a good tracer of the ISM abundances at the epoch of the PN progenitor formation. Recent studies have analyzed the circumstances that make the dredge-up of oxygen possible, both from theoretical and observational points of view.

Péquignot et al. (2000) argue that oxygen is a by-product of all third dredge-up, but leads to enrichment only at low metallicity. At solar metallicity, the dredged-up material has lower oxygen abundance than the original gas. Richer & McCall (2007) analyzed the abundances for a sample of bright PNe in nearby dwarf irregular galaxies. They suggest that the dredge-up of oxygen is an infrequent phenomenon also in low metallicity environment. Magrini et al. (2005a) and Kniazev et al. (2005) compared the chemical abundances of H II regions of the dwarf galaxy Sextans A with that of the PN known in this galaxy. Both authors found significant self-pollution of the PN progenitor, by a factor of ∼10 in oxygen. Leisy & Dennefeld (2006) found several examples of oxygen enrichment in the PNe of SMC, while their number was reduced in the LMC, which has a higher metallicity. Kniazev et al. (2007) found an enrichment in oxygen by 0.27±0.10 dex in the PN of the Fornax galaxy respect to the ISM. Finally, Kniazev et al. (2008) found that only one of the five PNe in the dwarf galaxy Sagittarius shows the effect of the third dredge-up. They argue that the different behavior respect to the remaining PN population of Sagittarius could be due to a different characteristic of the progenitor, such as the presence of rotation (Siess, Goriely & Langer 2004) and/or a different age (and thus mass).

In Figure 4 we study the presence or not of the third-dredge in a number of nearby dwarf irregular galaxies (or dwarf irregulars, dIrs). We do not plot the data for dwarf spheroidal galaxies since the comparison with the present-time ISM is not possible. The idea behind the comparison of PNe abundance ratios as a function of the oxygen abundance in different galaxies, with the 12+log(O/H) of the H II regions in each of these galaxies (vertical lines), and in a sample of BCGs ('horizontal' lines), is that in H II regions, the oxygen that is seen has been produced by the same massive stars that produced the alpha-process neon, sulfur and argon. Therefore, in this plot, log(Ne/O), log(S/O) and log(Ar/O) should be constant and show no dependence on the oxygen abundance. In fact, inspecting Figure 4 we see that in the three diagrams most of the PNe are distributed along the line that defines the BCGs abundance ratios of H II regions, thus with no trends with respect to the oxygen abundance. The oxygen production in these diagrams should have two effects: *i)* to place the PN points well ahead of the mean abundance in the ISM, *ii)* to de-

press the Ne/O, S/O, and Ar/O ratios, unless the production of Ne, S, and Ar also occurs. In a conservative view, we would aspect that the presence of both effects would probe the third-dredge-up occurrence. Few PNe pass this test full-filling both requests, usually with abundance ratios that are not completely understood. Note from the plot that for galaxies of much lower metallicity this contribution is important, as in the case of Sex A [12+log(O/H)=7.6] and NGC 3109 [12+log(O/H)=7.7] (see Ne/O and S/O, but also their displacement from the average ISM O/H). In fact, previous authors, when discussing the abundance patterns of the PN population of these two galaxies, have already pointed out this effect (Magrini et al. 2005a and Peña et al. 2007, respectively). Being less conservative, also some PNe of Sextans B, whose O/H abundances are ahead of the mean abundance in the ISM, could be affected by oxygen production. However, at the metallicity of IC10 [12+log(O/H)=8.3] we do not find important contributions of dredge-up in the abundance of oxygen: all PNe have O/H close to the present-time ISM one, and no particularly depressed Ne/O, Ar/O, and S/O ratios are observed.

Remembering, as discussed above, that the third dredge-up of oxygen is a metallicity dependent phenomenon, this kind of plots can also be useful to give a lower limit above of which no third dredge-up effect is seen in the nearby dwarf irregulars. So far, as determined by all the available data in the literature, this limit is around 12+log(O/H)=7.7.

8 SUMMARY AND CONCLUSIONS

In this paper we present imaging and spectroscopic observations of a sample of PNe and H II regions in the nearby starburst galaxy IC10. The pre-imaging observations allowed us to discover 12 new PNe in the central $5.5' \times 5.5'$ regions. We derived physical and chemical properties of 6 PNe (one of them with direct electron temperature measurement) and of 10 H II regions (7 with direct electron temperature). Using the PN Hα flux and the upper limit to the HeII/Hβ ratio we evaluated the mass and the formation epoch of the PN progenitors. From the analysis of the above properties of PNe and H II regions we found:

- in our rough age estimation, PN progenitors are coeval within few Gyr and were born between 7 and 10 Gyr ago;
- the mean oxygen abundances of PNe and H II regions are similar, indicating a small chemical enrichment;
- both from PNe and H II regions, the mean oxygen abundance is sub-solar, 12+log(O/H)=8.3;
- the metallicity of the interstellar medium was not homogeneous, neither at present-time (from H II regions) nor in the past (from PNe);
- the third-dredge up of oxygen does not occur in the PNe of IC10, and from a comparative analysis of PNe in dwarf irregular galaxies it seems to be allowed, but not mandatory, for 12+log(O/H)$\leqslant$7.7.

ACKNOWLEDGMENTS

We thank Michael Richer, the referee of this paper, for his careful reading of the manuscript and for his comments which improved the quality and the presentation of the paper. Two Brazilian and one Italian agency gave us partial support for this work. So DRG and LM would like to thank FAPESP for its grants: 2003/09692-0 and 2006/59301-6, respectively, and the FAPERJ's grant, E-26/110.107/2008.

REFERENCES

Asplund M., Grevesse N., Sauval A. J., 2005, ASPC, 336, 25
Benjamin R. A., Skillman E. D., & Smits D. P., 1999, ApJ 514, 307
Borissova J., Georgiev L., Rosado M., Kurtev R., Bullejos A., Valdez-Gutiérrez M., 2000, A&A 363, 130
Clegg R. E. S., 1987, MNRAS 229, 31
de Avillez M. A., Mac Low M.-M., 2002, ApJ, 581, 1047
Demers, S., Battinelli, P., & Letarte, B. 2004, A&A, 424, 125
Dopita M. A., 1991, IAUS, 148, 393
Drozdovsky I. O., Schulte-Ladbeck R. E., Hopp U., Greggio L., Crone M. M., 2002, AJ 124, 811
Garnett D. R., 1990, ApJ 363, 142
Gil de Paz, A., Zamorano, J., & Gallego, J. 2000, A&A, 361, 465
Gonçalves D. R., Magrini L., Munari U., Corradi R. L. M., & Costa R. D. D., 2008, MNRAS 391, L84
Hodge P., & Lee M. G., 1990, PASP 102, 26
Izotov Y. I., Stasinska G., Meynet G.,Guseva N. G., & Thuan T. X., 2006, A&A 448, 955
Kniazev A. Y., Grebel E. K., Pustilnik S. A., Pramskij A. G., Zucker D. B., 2005, AJ 130, 1558
Kniazev A. Y., Grebel E. K., Pustilnik S. A., & Pramskij A. G., 2007, A&A 468, 121
Kniazev A. Y., Pustilnik S. A., & Zucker D. B., 2008, MNRAS, 384, 1045
Kingsburgh R. L., & Barlow M. J., 1994, MNRAS 271, 257
Kobulnicky H. A., & Skillman E. D., 1996, ApJ 471, 211
Lee H., Skillman E. D., Cannon J. M., Jackson D. C., Gehrz R. D., Polomski E. F., Woodward C. E., 2006, ApJ, 647, 970
Leisy P. & Dennefeld M., 2006, A&A, 456, 451
Lequeux J., Peimbert M., Rayo J. F., Serrano A., Torres-Peimbert S. 1979, A&A 80, 155
López-Sánchez Á. R., Esteban C., 2008, A&A, 491, 131
Mac Low M.-M., Ferrara A., 1999, ApJ, 513, 142
Magrini L., Corradi R. M. L., Greimel R., Leisy P.; & Lennon D. J., 2003, A&A 407, 51
Magrini L. Leisy P., Corradi R. M. L., Perinotto M., Mampaso A. & Vílchez J. M., 2005a, A&A 443, 115
Magrini L., et al., 2005b, MNRAS, 361, 517
Magrini L., Stanghellini L., Villaver E., 2009, arXiv, arXiv:0901.2273, ApJ in press
Marigo P., 2001, A&A, 370, 194
Massey P., Strobel K., Barnes J. V., & Anderson E., 1988, ApJ, 328, 315
Massey P., Gronwall C., 1990, ApJ, 358, 344
Massey P., Armandroff T. E., & Conti P. S., 1992, AJ 103, 1159
Massey P., & Armandroff T. E., 1995, AJ 109, 2470
Mateo M. L., 1998, ARA&A 36, 435
Mathis J.S. 1990, ARA&A 28, 37

Melisse J. P. M., & Israel F. P., 1994, A&AS 103,391
Méndez R. H., Kudritzki R. P., Herrero A., 1992, A&A, 260, 329
Osterbrock D.E., Ferland G., 2006, Astrophysics of Gaseous Nebulae and Active Galactic Nuclei, 2nd. ed. (Univ. Science Books)
Peña M., Stasińska G., & Richer M. G., 2007, A&A 476, 745
Péquignot D., Walsh J. R., Zijlstra A. A., Dudziak G., 2000, A&A 361, L1
Pilyugin L. S., Thuan T. X., Vílchez J. M., 2003, A&A, 397, 487
Recchi, S., Spitoni, E., Matteucci, F., & Lanfranchi, G. A. 2008, A&A, 489, 555
Richer M. G., Bullejos A., Borissova J., McCall M. L., Lee H., Kurtev R., Georgiev L., Kingsburgh R. L., Ross R., & Rosado M., 2001, A&A 370, 34
Richer M. G., & McCall M. L., 2007, ApJ 658, 328
Sakai S., Madore B. F., Freedman W. L., 1999, ApJ, 511, 671
Sanna N., et al., 2008, ApJ, 688, L69
Sanna N., et al., 2008, arXiv:0905.2580
Skillman E. D., Kennicutt R. C., Hodge P. W., 1989, ApJ, 347, 875
Shostak G. S., & Skillman E. D., 1989, A&A 214, 33
Shaw R. A., & Dufour R. J., 1994, ASPC, 61, 327
Siess L., Goriely S., & Langer N., 2004, A&A 415, 1089
Stanghellini L., 2008, Proceedings of the IAU Symposium 256, The Magellanic System; van Loon abd Oliveira (Eds.)arXiv, arXiv:0810.4167
Stanghellini L., Guerrero M. A., Cunha K., Manchado A., Villaver E., 2006, ApJ, 651, 898
Stasińska G., 1990, A&AS, 83, 501
Thronson H. A., Jr., Hunter D. A., Casey S., Harper D. A., 1990, ApJ, 355, 94
Tsamis Y. G., & Péquignot D., 2005, MNRAS 364, 687
van den Hoek L. B., Groenewegen M. A. T., 1997, A&AS, 123, 305
Wilcots E. M., & Miller B. W., 1998, AJ 116, 2363

APPENDIX A: EMISSION-LINE FLUX MEASUREMENTS

In this section we present the observed emission-line fluxes and extinction corrected intensities measured in the samples of PNe and H II regions of IC10.

Table A1. Observed and extinction corrected fluxes of PNe. Column (1) gives the PN name; column (2) gives the observed Hβ flux in units of 10^{-17}erg cm^{-2} s^{-1}; column (3) the nebular extinction coefficient; columns (4) and (5) indicate the emitting ion and the rest frame wavelength in Å; columns (6), (7), and (8) give the measured (F_λ), the relative error on the measured fluxes (ΔF_λ) and the extinction corrected (I_λ) intensities. Both F_λ and I_λ are normalized to Hβ=100. Upper limits on the line fluxes are marked with :.

Id	$F_{H\beta}$	c(Hβ)	Ion	λ (Å)	F_λ	ΔF_λ	I_λ
IC10PN5	1.3	1.95	[OIII]	4363	9:	-	16.7
			HeII	4686	9:	-	10.7
			HI	4861	100.0	08%	100.
			[OIII]	4959	441.0	06%	395.
			[OIII]	5007	1384.	05%	1179.
			HeI	5876	47.0	10%	18.6
			[NII]	6548	43.5	10%	11.2
			HI	6563	1113.	06%	285.
			[NII]	6584	129.0	08%	32.6
			HeI	6678	16.7	12%	4.0
			[SII]	6717	15.3	12%	3.5
			[SII]	6731	13.2	12%	3.0
			HeI	7065	35.1	10%	6.6
			[ArIII]	7135	59.4	9.5%	10.6
			[SIII]	9069	65.6	9.0%	3.5
IC10PN9	3.7	1.49	[OIII]	4363	9:	-	9:
			HeII	4686	3:	-	3:
			HI	4861	100.	08%	100.
			[OIII]	4959	521.	05%	482.
			[OIII]	5007	1551.	04%	1375.
			[NII]	6548	33.	09%	12.
			HI	6563	809.	05%	285.
			[NII]	6584	98.7	08%	34.5
			HeI	6678	13.53	10%	4.54
			[SII]	6717	6.3	11%	2.0
			[SII]	6731	11.9	10%	3.9
			HeI	7065	39.49	09%	10.9
			[ArIII]	7135	38.9	09%	10.4
			[OII]	7320	24.81	10%	6.1
			[OII]	7330	36.0	09%	8.8
PN17	6.4	1.18	HI	4340	19.0	26%	27.2
			[OIII]	4363	5.5	28%	7.7
			HeII	4686	7.3	-	8.2
			HI	4861	100.00	16%	100.
			[OIII]	4959	166.2	14%	155.
			[OIII]	5007	473.4	09%	429.
			HeI	5876	29.3	22%	16.7
			[NII]	6548	31.0	22%	13.6
			HI	6563	653.	12%	285.
			[NII]	6584	96.7	22%	41.9
			[SII]	6731	13.8	28%	5.8
			HeI	6678	7.6	26%	3.1
			HeI	7065	15.8	23%	5.7
			[OII]	7320	23.5	23%	7.7
			[OII]	7330	20.5	22%	6.7
			[SIII]	9069	30.3	22%	8.2
PN20	2.1	1.89	[OIII]	4363	5:	-	9:
			HI	4861	100.0	10%	100.0
			[OIII]	4959	409.	09%	368.
			[OIII]	5007	1236.	06%	1061.
			HeI	5876	24.6	13%	10.0
			[NII]	6548	58.3	12%	15.7
			HI	6563	1070.	06%	285.
			[NII]	6584	177.	9.5%	46.5
			HeI	6678	21.	13%	5.3
			[SII]	6717	33.4	13%	8.1
			[SII]	6731	53.0	12%	12.8
			HeI	7065	32.9	13%	6.7
			[ArIII]	7135	68.7	11%	12.9
			[SIII]	9069	53.8	12%	18.3

Table A1 – *continued*

Id	$F_{H\beta}$	c(Hβ)	Ion	λ (Å)	F_λ	ΔF_λ	I_λ
PN21	3.1	1.06	[OIII]	4363	6:	-	7.8
			HI	4861	100.	22%	100.
			[OIII]	4959	141.	22%	133.
			[OIII]	5007	539.	19%	496.
			[NII]	6548	88.5	22%	42.
			HI	6563	599.	18%	285.
			[NII]	6584	275.	20%	130.
			HeI	6678	14.2	23%	8.6
			[SII]	6717	26.4	23%	11.9
			[SII]	6731	39.3	23%	17.7
			[ArIII]	7135	29.2	23%	11.5
			[SIII]	9069	49.4	22%	10.0
PN22	3.5	1.65	[OII]	3727	198.	12%	577.
			[OIII]	4363	14:	-	22:
			HeII	4686	10:	-	12:
			HI	4861	100.	13%	100.
			[OIII]	4959	445.	10%	409.
			[OIII]	5007	1415.	06%	1241.
			HeI	5876	25.	06%	11.
			[NII]	6548	61.7	13%	19.6
			HI	6563	904.	06%	285.
			[NII]	6584	162.	12%	50.5
			[SII]	6717	9.4	21%	2.7
			[SII]	6731	15.5	20%	4.5
			HeI	7065	42.6	16%	10.3
			[ArIII]	7135	67.2	13%	15.6
			[SIII]	9069	80.2	13%	6.7
PN23	0.55	1.48	HeII	4686	19:	-	23:
			HI	4861	100.	24%	100.
			[OIII]	4959	69.6	28%	64.
			[OIII]	5007	164.	20%	145.
			[NII]	6548	113.	20%	41.
			HI	6563	801.	10%	285.
			[NII]	6584	341.	17%	120.
			[SII]	6717	46.2	28%	15.3
			[SII]	6731	36.1	30%	11.9
			HeI	7065	9.8	36%	2.8
PN24	3.7	1.41	HI	4861	100.	09%	100.
			[OIII]	4959	611.	06%	565.
			[OIII]	5007	1780.	05%	1601.
			HeI	5876	57.	09%	29.
			[NII]	6548	60.	09%	22.5
			HI	6563	764.	5.5%	285.
			[NII]	6584	169.	07%	62.5
			[SII]	6731	32.1	9.5%	11.1
			[ArIII]	7135	59.9	09%	17.2
PN25	0.22	0.92	HI	4861	100.	12%	100.
			[OIII]	4959	386.	10%	367.
			[OIII]	5007	1140.	06%	1058.
			HI	6563	544.	11%	285.

Table A2. Observed and de-reddened fluxes of H II regions. Column (1) gives the name of the H II region. The rest of the columns are as in Table 2.

ID	$F_{H\beta}$	c(Hβ)	Ion	λ (Å)	F_λ	ΔF_λ	I_λ
IC10PN7	111	1.63	[OII]	3727	35.45	07%	101.
			[NeIII]	3869	5.05	11%	12.7
			[NeIII]/HI	3968	7.53	10%	17.2
			HI	4100	10.4	09%	21.1
			HI	4340	27.8	6.5%	45.2
			[OIII]	4363	1.9:	-	3.5:
			HI	4861	100.	05%	100.
			[OIII]	4959	148.	4.5%	135.
			[OIII]	5007	455.	03%	397.
			HeI	5876	25.3	6.5%	11.7
			[OI]	6300	3.74	10%	1.38
			[OI]	6363	3.22	10%	1.15
			[NII]	6548	25.2	6.5%	8.15
			HI	6563	889.	05%	285.
			[NII]	6584	76.2	03%	24.1
			HeI	6678	13.2	05%	4.01
			[SII]	6717	39.8	9.5%	11.8
			[SII]	6731	32.1	6.5%	9.43
			HeI	7065	9.42	6.5%	2.32
			[ArIII]	7135	48.5	6.5%	11.5
			[OII]	7320	8.72	09%	1.88
			[OII]	7330	6.98	09%	1.50
			[ArIII]	7751	11.9	9.5%	2.07
			[SIII]	9069	67.2	06%	5.81
HL90-13	-	0.04	HI	4861	100.	05%	100.
			[OIII]	4959	110.	05%	110.
			[OIII]	5007	327.	04%	326.
			HeI	5876	9.53	08%	9.36
			[NII]	6548	7.99	08%	7.78
			HI	6563	292.	04%	285.
			[NII]	6584	25.1	07%	24.5
			HeI	6678	3.68	09%	3.68
			[SII]	6717	20.4	07%	19.8
			[SII]	6731	16.0	07%	15.5
			[ArIII]	7135	20.7	07%	20.1
			[OII]	7320	5.67	09%	5.48
			[OII]	7330	3.99	09%	3.85
			[ArIII]	7751	5.74	09%	5.51
			[SIII]	9069	36.0	06%	34.0
HL90-20	-	1.34	[OII]	3727	42.1	09%	100.
			[NeIII]	3968	6.04	14.5%	12.0
			HI	4100	13.5	14.5%	24.3
			HI	4340	33.0	09%	49.4
			[OIII]	4363	2.71:	-	4.20:
			HeI	4471	3.12	15%	4.21
			HI	4861	100.	08%	100.
			[OIII]	4959	118.	08%	110.
			[OIII]	5007	379.	06%	341.
			HeI	5876	24.8	10%	13.1
			[NII]	6548	15.3	14.5%	6.05
			HI	6563	726.	05%	285.
			[NII]	6584	41.5	09%	16.1
			HeI	6678	11.8	14.5%	4.47
			[SII]	6717	26.9	10%	9.91
			[SII]	6731	20.8	11%	7.61
			HeI	7065	7.85	15%	2.48
			[ArIII]	7135	36.5	09%	11.2
			[OII]	7320	5.05	15%	1.43
			[OII]	7330	3.82	15%	1.08
			[ArIII]	7751	9.42	14%	2.23
			[SIII]	9069	73.3	07%	9.86

Table A2 – *continued*

ID	$F_{H\beta}$	c(Hβ)	Ion	λ (Å)	F_λ	ΔF_λ	I_λ
HL90 29	128	1.22	[OII]	3727	110.	13%	244.
			HI	4340	36.1	19%	52.2
			[OIII]	4363	8.33	28%	14.5
			HI	4861	100.	13%	100.
			[OIII]	4959	254.	09%	238.
			[OIII]	5007	742.	06%	673.
			HeI	5876	32.1	19%	17.9
			[NII]	6548	40.4	18%	17.3
			HI	6563	670.	06%	285.
			[NII]	6584	90.4	12%	38.1
			[SII]	6717	99.0	11%	39.6
			[SII]	6731	74.0	13%	29.4
			[ArIII]	7135	56.1	17%	19.1
			[OII]	7320	9.20	23%	2.91
			[OII]	7330	8.74	23%	2.74
			[ArIII]	7751	13.6	21%	3.64
			[SIII]	9069	49.0	13%	11.8
HL90-30	110	1.63	HI	4340	28.5	18%	46.5
			[OIII]	4363	3.00:	-	4.8:
			HI	4861	100.	14%	100.
			[OIII]	4959	116.	14%	106.
			[OIII]	5007	407.	13%	357.
			HeI	5876	29.5	18%	13.5
			[NII]	6548	25.1	18%	8.13
			HI	6563	894.	12%	286.
			[NII]	6584	65.4	14%	20.7
			HeI	6678	12.7	17%	3.84
			[SII]	6717	48.9	15%	14.4
			[SII]	6731	39.6	15%	11.6
			[ArIII]	7135	49.1	15%	11.6
			[OII]	7320	9.57	17%	2.06
			[OII]	7330	8.04	17%	1.72
			[ArIII]	7751	11.5	17%	1.98
			[SIII]	9069	81.4	14%	6.98
HL90-40	10.3	1.43	[OII]	3727	106.	05%	270.
			HI	4340	22.7	17%	35.0
			HI	4861	100.	05%	100.
			[OIII]	4959	50.5	14%	46.9
			[OIII]	5007	153.6	09%	137.
			HeI	5876	24.0	17%	12.1
			[OI]	6300	9.17	20%	3.82
			[NII]	6548	38.8	15%	14.4
			HI	6563	777.	04%	286.
			[NII]	6584	110.	06%	40.1
			HeI	6678	13.3	20%	4.66
			[SII]	6717	142.	05%	48.7
			[SII]	6731	98.1	05%	33.4
			HeI	7065	5.42	23%	1.58
			[ArIII]	7135	25.2	17%	7.14
			[SIII]	9069	41.7	15%	4.84

Table A2 – *continued*

ID	$F_{H\beta}$	c(Hβ)	Ion	λ (Å)	F_λ	ΔF_λ	I_λ
HL90-45 (BR1)	1025.	1.81	[OII]	3727	31.0	26%	100.
			HI	3835	2.30	30%	6.69
			[NeIII]	3869	16.6	26%	46.6
			HeI	3889	6.67	30%	18.3
			[NeIII]/HI	3968	12.0	26%	30.4
			HI	4100	12.4	26%	27.5
			HI	4340	30.8	24%	53.1
			[OIII]	4363	2.84	30%	4.78
			HeI	4471	3.17	30%	4.76
			HeI/[ArIV]	4712	0.79	35%	0.93
			[ArIV]	4740	0.24	35%	0.27
			HI	4861	100.	19%	100.
			[OIII]	4959	275.	13%	251.
			[OIII]	5007	874.	11%	757.
			[NII]	5755	0.32	35%	0.14
			HeI	5876	33.7	24%	14.2
			[OI]	6300	3.33	30%	1.09
			[OI]	6363	0.85	35%	0.27
			[NII]	6548	10.0	26%	2.86
			HI	6563	1012.	11%	285.
			[NII]	6584	35.5	24%	9.89
			HeI	6678	15.1	26%	4.02
			[SII]	6717	25.2	25%	6.50
			[SII]	6731	24.7	25%	6.33
			HeI	7065	20.6	26%	4.37
			[ArIII]	7135	60.7	20%	12.3
			[ArIII]	7751	18.6	26%	2.64
HL90-50	880.	1.52	[OII]	3727	43.0	08%	115.
			[NeIII]	3869	8.31	11%	19.6
			HeI	3889	8.28	11%	19.2
			[NeIII]/HI	3968	9.47	11%	20.5
			HI	4100	18.8	09%	36.5
			HI	4340	39.7	08%	62.6
			[OIII]	4363	2.71	10%	4.20
			HeI	4471	4.22	13%	5.94
			HI	4861	100.	07%	100.
			[OIII]	4959	130.	06%	120.
			[OIII]	5007	390.	04%	344.
			HeI	5876	33.5	08%	16.3
			[OI]	6300	1.06	14%	0.42
			[NII]	6548	17.4	04%	6.09
			HI	6563	823.	08%	285.
			[NII]	6584	48.5	08%	16.6
			[SII]	6717	31.5	09%	10.1
			[SII]	6731	24.9	09%	7.96
			HeI	7065	8.56	08%	2.32
			[ArIII]	7135	48.1	11%	12.6
			[OII]	7320	6.88	11%	1.65
			[OII]	7330	6.39	09%	1.52
			[ArIII]	7751	12.7	09%	2.48
			[SIII]	9069	49.0	08%	5.03
HL90-51	47.	1.88	HI	4100	20.4	16%	46.4
			HI	4340	25.5	15%	44.9
			[OIII]	4363	2:	-	4.1
			HI	4861	100.	10%	100.
			[OIII]	4959	151.	09%	137.
			[OIII]	5007	397.	05%	340.
			HeI	5876	26.1	15%	10.7
			[OI]	6300	2.6	20%	1.
			[NII]	6548	22.7	16%	6.2
			HI	6563	1063.	07%	285.
			[NII]	6584	71.3	11%	19.
			[SII]	6717	51.2	12%	12.6
			[SII]	6731	47.8	12%	11.7
			HeI	7065	21.6	16%	4.3
			[ArIII]	7135	63.1	11%	12.
			[OII]	7320	16.2	16%	2.8
			[OII]	7330	9.81	17%	1.7
			[ArIII]	7751	17.7	16%	2.3
			[SIII]	9069	115.	10%	8.9

Table A2 – *continued*

ID	$F_{H\beta}$	c(Hβ)	Ion	λ (Å)	F_λ	ΔF_λ	I_λ
HL90-107	57.	1.74	HI	4340	21.2	8.5%	35.7
			[OIII]	4363	5.6:	-	9.3:
			HI	4861	100.	06%	100.
			[OIII]	4959	285.	05%	261.
			[OIII]	5007	862.	03%	751.
			HeI	5876	26.9	08%	11.7
			[OI]	6300	12.7	8.5%	4.39
			[OI]	6363	4.95	10%	1.64
			[NII]	6548	22.4	08%	6.70
			HI	6563	963.	03%	285.
			[NII]	6584	70.2	06%	20.5
			HeI	6678	13.8	8.5%	3.90
			[SII]	6717	100.	06%	27.8
			[SII]	6731	79.3	06%	21.7
			HeI	7065	14.4	8.5%	2.49
			[ArIII]	7135	75.8	06%	16.3
			[OII]	7320	8.30	8.5%	1.60
			[OII]	7330	8.19	8.5%	1.60
			[ArIII]	7751	18.4	08%	2.82
			[SIII]	9069	98.9	06%	7.33
HL90-111	4300.	1.05	[OII]	3727	71.6	08%	141.
			HI	4340	26.5	10%	36.3
			[OIII]	4363	0.93:	-	1.26:
			HI	4861	100.	06%	100.
			[OIII]	4959	65.7	08%	62.2
			[OIII]	5007	196.5	4.5%	180.
			HeI	5876	18.0	10%	10.9
			[NII]	6548	19.3	10%	9.33
			HI	6563	593.	04%	285.
			[NII]	6584	57.0	08%	27.1
			HeI	6678	8.56	13%	3.96
			[SII]	6717	37.1	8.5%	16.9
			[SII]	6731	28.0	10%	12.7
			HeI	7065	5.97	13%	2.42
			[ArIII]	7135	31.4	13%	12.4
			[OII]	7320	7.15	13%	2.66
			[OII]	7330	5.92	13%	2.19
			[ArIII]	7751	8.43	13%	2.72
HL90-120	108.	0.40	[OII]	3727	41.6	11%	48.4
			HI	3835	3.22	16%	3.70
			[NeIII]	3869	14.9	13%	17.0
			HeI	3889	9.45	14%	10.7
			[NeIII]/HI	3968	13.9	13%	15.7
			HI	4100	16.1	13%	17.9
			HI	4340	36.1	11%	38.7
			[OIII]	4363	1.69	16%	1.81
			HeI	4471	3.60	16%	3.80
			HeII	4686	4.82	16%	4.94 [a]
			HI	4861	100.	10%	100.
			[OIII]	4959	149.	10%	147.
			[OIII]	5007	378.	09%	370.
			HeI	5876	5.89	16%	5.27
			[OI]	6300	1.27	16%	1.10
			[SIII]	6312	1.54	16%	1.2
			[NII]	6548	6.95	15%	5.3
			HI	6563	376.	09%	285.
			[NII]	6584	23.0	12.5%	17.4
			HeI	6678	2.31	16%	1.7
			[SII]	6717	12.9	13%	9.7
			[SII]	6731	9.55	14%	7.1
			HeI	7065	1.51	16%	1.1
			[ArIII]	7135	9.54	14%	6.7
			[OII]	7320	2.23	16%	1.5
			[OII]	7330	1.73	16%	1.2

[a] Stellar broad line emission from WR stars

Table A2 – *continued*

ID	$F_{H\beta}$	c(Hβ)	Ion	λ (Å)	F_λ	ΔF_λ	I_λ
HL90-122	61.	1.04	HI	4340	29.7	10%	40.6
			HI	4861	100.	09%	100.
			[OIII]	4959	21.6	11%	20.4
			[OIII]	5007	64.7	9.5%	59.5
			HeI	5876	5.97	16%	3.64
			[NII]	6548	30.2	10%	14.7
			HI	6563	591.	06%	286.
			[NII]	6584	93.5	09%	44.9
			HeI	6678	4.48	17%	2.08
			[SII]	6717	61.9	9.5%	28.4
			[SII]	6731	45.6	10%	20.8
			HeI	7065	3.24	18%	1.33
			[ArIII]	7135	16.1	11%	6.44
			[OII]	7320	5.16	16%	1.94
			[OII]	7330	5.64	16%	2.11
HL90-127	12.4	1.10	HI	4340	26.5	10%	36.9
			HI	4861	100.	07%	100.
			[OIII]	4959	158.	06%	150.
			[OIII]	5007	477.	05%	437.
			HeI	5876	21.3	10%	12.6
			[NII]	6548	9.49	12%	4.43
			HI	6563	616.	04%	285.
			[NII]	6584	29.2	10%	13.4
			HeI	6678	12.1	12%	5.42
			[ArIII]	7135	35.3	09%	13.3
HL90-141	48.7	1.23	HI	4340	26.7	15%	38.7
			HI	4861	100.	08%	100.
			[OIII]	4959	66.7	08%	62.6
			[OIII]	5007	210.	05%	190.
			[NII]	6548	22.0	15%	9.38
			HI	6563	675.	05%	286.
			[NII]	6584	87.3	08%	36.6
			HeI	6678	9.00	18%	3.64
			[SII]	6717	64.2	08%	25.5
			[SII]	6731	44.5	09%	17.6
			[ArIII]	7135	24.0	15%	8.12
			[OII]	7320	5.64	25%	1.77
			[OII]	7330	9.62	18%	3.00